Applied Ocean Research 99 (2020) 102162

Contents lists available at ScienceDirect

Applied Ocean Research

journal homepage: www.elsevier.com/locate/apor

Effect of roughness in full-scale validation of a CFD model of self-propelled ships

Henrik Mikkelsen[a], Jens Honoré Walther[a,b]

[a] Technical University of Denmark, Department of Mechanical Engineering, Nils Koppels Allé, Building 404, 2700 Kgs. Lyngby, Denmark
[b] Swiss Federal Institute of Technology Zurich, Computational Science & Engineering Laboratory, Clausiusstrasse 33, CH-8092 Switzerland

ARTICLE INFO

Keywords:
CFD
Full-scale ship propulsion
Speed trial validation
Self-propulsion simulation
Roughness

ABSTRACT

This paper presents a comparison of full-scale computational fluid dynamics (CFD) simulations with speed trial measurements for a ro-ro vessel and a general cargo vessel. Significant work has been done on validating CFD simulation in model scale. However, in full-scale very few publicly available studies have been conducted due to limited access of validation data. The present study includes extensive validation and verification of both resistance, propeller open-water and self-propulsion simulations in both model and full-scale. The self-propulsion simulations include modelling of the free surface and rotation of the 3D propeller. Full-scale resistance and propeller open-water as well as model scale self-propulsion simulations show good agreement with towing tank measurements and predictions. However, the full-scale self-propulsion simulations using the traditional approach of including the roughness as a point force estimated by an empirical formula significantly underestimate the power from the speed trial measurements. By including the effect of hull and propeller roughness directly into the CFD model, by modifying the wall functions, the discrepancy between CFD and speed trial measurements decreases significantly. This indicates that inclusion of a roughness model directly into the CFD simulation could be a more accurate method than the traditional approach of using empirical formulas originally designed for towing tank extrapolation.

1. Introduction

Traditionally, the performance of a ship design is predicted by conducting towing tank experiments on a downscaled version of the ship (model scale). The results from these towing tank tests are then extrapolated to the scale of the actual ship (full-scale). An alternative to testing in a towing tank is to numerically simulate the flow around the ship using computational fluid dynamics (CFD). CFD simulations can be performed in full-scale, eliminating scale effects and the need for extrapolation. However, a disadvantage of using CFD is the modelling errors e.g. free surface and turbulence models.

Towing tank testing is expensive and waiting time for a slot can be significant. Many design iterations are needed with the increasing demand for fuel efficiency from the shipowners' contractual requirements and from regulation such as the Energy Efficiency Design Index (EEDI) requirements from the International Maritime Organization [1]. Testing of multiple hull designs in the towing tank is very time-consuming and costly since a new wooden model needs to be manufactured for each design. When using CFD, the design can be changed very quickly in the CAD software. It can even be done without human interaction if a fully automated design procedure is made by coupling the CFD code with a parametric CAD model and an optimization algorithm tool. The user will only need to specify the design exploration space and one or multiple objectives, such as minimum power for a speed profile or minimum EEDI. After the optimal design has been found, the geometry can be tested and validated in the towing tank.

Validation and verification of CFD simulations are important. Much work has been done on validating model scale CFD simulations by comparing with towing tank measurements, cf. e.g. Kim et al. [2], which showed good agreement with experimental results of the research ship Kriso Container Ship (KCS). Furthermore, validation workshops have been hosted where the participants submit CFD results to be compared with towing tank results [3,4]. The conclusions from these workshops are that carefully conducted CFD simulations can accurately estimate the resistance and performance of model scale ships. The next step is validation of full-scale CFD simulations. However, very few publicly available studies have been conducted due to limited access of validation data. A large contribution to full-scale validation is the Lloyd's Register (LR) workshop from 2016 [5]. The participants of the workshop blindly submitted twenty-four sets of full-scale self-propulsion calculations. It is important to note that the LR workshop participants used a wide range of methods and some have including

E-mail address: jhw@mek.dtu.dk (J.H. Walther).

https://doi.org/10.1016/j.apor.2020.102162
Received 7 November 2019; Received in revised form 7 April 2020; Accepted 10 April 2020

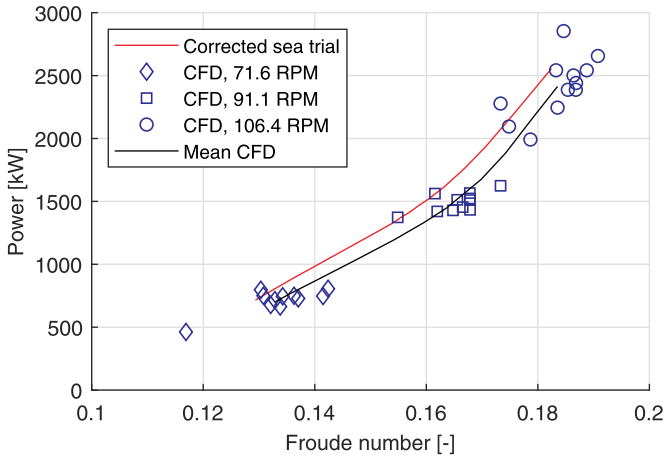

Fig. 1. Comparison of CFD results from workshop participants and speed trial measurements for the LR workshop vessel REGAL.[5]

roughness and air resistance and some have not. The comparison of the submitted CFD results with the speed trial measurements is shown in Fig. 1.

As seen, some of the CFD results show good agreement with the speed trial measurements, and some show large descrepancies. However, in average the CFD simulations underpredict the power. In CFD workshops in model scale [3,4], the participants in general obtain a much more accurate power prediction. The main difference between model-scale and full-scale is the roughness of the hull and propeller, wind loads on the superstructure and the difference in Reynolds number. Another comparison between full-scale CFD and speed trial measurements of a car carrier has been conducted by Jasak et al. [6] using an actuator disc to model the propeller showing apparent good correspondence. For both studies [5,6], the speed trial data were for a single ship. In the present study, the speed trial reference is based on the average of six sister vessels. The conducted self-propulsion CFD simulations in this study include the geometric propeller. A third full-scale validation study conducted by Mikkelsen et al. [7] showed that full-scale CFD and towing tank predictions had similar accuracy in prediction of the delivered power from the speed trial. However, in this study the sea trial power measurement was obtained from an inaccurate engine formula. The study by Sun et al. [8] compares model tank test, CFD simulations and speed trial for a bulk carrier. Both the studies by Mikkelsen et al. [7] and Sun et al. [8] does not resolve the surface. Instead, a double body approach is used and a correction is added for account for free surface effect.

When predicting the full-scale performance of a vessel, the resistance from surface roughness is very important. Even for new ships with little or no biofouling, the paint roughness, welding seams, variation in plate thickness etc. increase the hull resistance. In the present study, the effects of full-scale hull and propeller roughness is implemented and compared using two different approaches, and comparisons will be made. The traditional approach is using empirical formulas to predict the roughness and apply it as a concentrated point force. The alternative method is to account for the surface roughness by modifying the wall functions in the turbulence model as proposed by Cebeci and Bradshaw [9]. By modifying the wall functions, the boundary layer thickness is increased, which increases the wake field fraction as shown by Song et al. [10]. A validation study in model scale by Song et al. [11] showed good agreement between the CFD with modified wall functions and a towing tank experiment of a ship with a rough hull. The effect of biofouling has been studies by Song et al. [12], who using CFD studied the effect of biofouling on the self-propulsion parameters and propulsive efficiencies. To the authors' knowledge, the present study is the first where speed trial measurements are compared with full-scale CFD simulations with geometrically rotating propeller, resolved free surface and hull and propeller roughness modelled using a modified wall function approach.

Table 1
Principal particulars of the general cargo ship.

Length p.p.	L_{PP}	138m
Beam	B	23.00m
Draft	TA/TF	5.6m/4.9m
Design dead weight	$DW_{Scantling}$	16, 890DWT

The paper starts with a short presentation of the studied vessels and measurements in Sec. 2 followed by Sec. 3 describing the methods and CFD set-up in detail. In Sec. 4, the results are presented and discussed. Finally, conclusions are drawn in Sec. 5.

2. The studied vessel and measurements

In the present study, two vessels are studied. The main study involves an approximately 200m ro-ro vessel built by a European shipyard where six sister vessels of the same design have been built. Since towing tank tests and speed trial test has been conducted on vessel, it can be used to study resistance, propulsion and scale effects separately. However, only limited data can be shared about this vessel due to confidentiality agreements. To include an open source vessel, a secondary vessel is studied. The secondary vessel is the 138m general cargo vessel REGAL used for the 2016 LR Workshop on Ships Scale Hydrodynamics Computer Simulation [5]. The principal particulars of the vessel are shown in Table 1. The REGAL vessel is to the authors' knowledge the only case where all necessary geometry and speed trial data are publicly available. The general cargo vessel will only be considered in Sec. 4.3.1. The geometries consist of a hull, rudders, and propellers. The ro-ro vessel geometry also consists of appendages.

2.1. Hull

The ro-ro hull including rudders and shaft arrangements has been provided as a 3D geometry by the shipyard. The effect of the bilge keel is neglected in the study since it is small for this vessel. The displacement of the vessels during the speed trials condition is approximately 70% of the displacement in the design condition. All comparisons will be conducted in sea trial condition. The vessels are sailing at a Reynolds number $\mathrm{Re} = \frac{UL_{PP}}{\nu}$ of approximately and a Froude number $\mathrm{Fn} = \frac{U}{\sqrt{gL_{PP}}}$ of approximately $0.2 - 0.3$, where U is the vessel speed, L_{PP} is the length between perpendiculars, ν is the kinematic viscosity of the water and g is the gravitational acceleration.

2.2. Propeller

The geometries of the four bladed controllable pitch propellers for the ro-ro vessel used in the towing tank test and the ones manufactured to the actual vessels are slightly different. Both propeller designs have been delivered as a 3D geometry by the propeller manufacturer. The CFD simulations in model scale have been conducted with the propeller geometry used in the towing tank. However, the full-scale CFD simulations have been conducted with the propeller geometry which is used to manufacture the propellers to the actual vessels.

2.3. Towing tank testing

Towing tank tests of the vessel have been conducted by Hamburgische Schiffbau-Versuchsanstalt GmbH (HSVA) in Hamburg, Germany. The test types conducted by the towing tank are resistance tests, propeller open-water tests and self-propulsion. The measurements from the towing tank have been extrapolated to full-scale predictions by HSVA using confidential in-house correlations. Only one set of towing tank tests have been conducted for the vessel, since the hull and

propellers are the same for the sister vessels.

2.4. Speed trial

Speed trials have been conducted for each of the six sister vessels. In 2015, IMO and ITTC released ISO15016:2015 [13], which is an updated version of the ISO 15016:2002 standard procedure for carrying out and correcting speed trials. The speed trials of all vessels has been conducted according to the ISO15016:2015 standard [13].

The main measurements at the speed trials are speed, propeller rate of rotation, and the delivered power to the propeller.

2.4.1. Speed measurement and corrections

The speed of the vessel during the speed trial is measured using a GPS. From the GPS data, the ship speed over ground is calculated, and a mean is calculated by assuming no lateral drift.

The wave height and direction were estimated by visual observations and agreed upon on the bridge during the speed trial with representatives from both captain, owner, classification society and yard.

2.4.2. Power measurement and correction

The delivered power is calculated from strain gauges mounted on the shafts. The strain gauges are of the type 3/350LE VY11S-3 by HBM. The strain gauges are mounted for the sole purpose of the speed trial. The mounting and power analysis have been conducted by DNV GL as a third party.

Corrections due to wind, waves, current, water salinity, water temperature and deviating displacement have been conducted after the speed trial as specified in ISO15016:2015 [13].

3. Computational fluid dynamics

This section describes the CFD set-ups developed and used in this study. All the CFD simulations are performed in the commercial CFD-code STAR-CCM+ v.2019.1.1 from Siemens [14]. STAR-CCM+ discretizes the governing equations using an unstructured finite-volume method. The code is widely used in the marine industry and is well-known for its capabilities within marine applications.

In total three CFD set-ups are developed: resistance set-up, propeller open-water set-up, and self-propulsion set-up. All set-ups are used in both model and full-scale.

The used computational power and number of cells for calculating one speed for the different test types can be seen in Table 2.

3.1. Governing equations and CFD output

The governing equations of an incompressible Newtonian fluid are the Navier-Stokes equations [15]:

$$\frac{\partial u_i}{\partial x_i} = 0 \tag{1}$$

$$\rho\frac{\partial u_i}{\partial t} + \rho u_j\frac{\partial u_i}{\partial x_j} = -\frac{\partial p}{\partial x_i} + \frac{\partial}{\partial x_j}(2\mu S_{ij} - \rho\overline{u_j' u_i'}) \tag{2}$$

where u_i is the velocity vector, t is time, p is pressure, μ is dynamic viscosity, $S_{ij} = \frac{1}{2}\left(\frac{\partial u_i}{\partial x_j} + \frac{\partial u_j}{\partial x_i}\right)$ is the mean strain rate, and u_i' is the turbulent fluctuating part of the velocity.

In order to close the problem the Reynolds stresses are modelled using a linear eddy viscosity model. The linear constitutive relationship [16] is:

$$-\rho\overline{u_i' u_j'} = 2\mu_t S_{ij} - \frac{2}{3}\rho k\delta_{ij} \tag{3}$$

where μ_t is the turbulent viscosity, k is the turbulent kinetic energy, and δ_{ij} is Kronecker's delta.

In this study, besides the model scale propeller open-water simulations, the turbulent viscosity is calculated using the realisable $k-\epsilon$ turbulence model [14,17]. The $k-\epsilon$ model is a two equations model using k and the turbulent dissipation rate ϵ [16]:

$$\mu_t = \rho C_\mu \frac{k^2}{\epsilon} \tag{4}$$

where C_μ is a combination of constants and available flow parameters.

For the propeller open-water simulations in model scale, the actual flow on the propeller blade goes from laminar regime to transitionally turbulent and finally to fully turbulent. The turbulence model is derived assuming a fully turbulent flow. In order to model the influence of transition, the Gamma ReTheta approach is used [14,18]. This adds the two transport equations for the intermittency and transition momentum thickness Reynolds number. The model scale propeller open-water simulations use the $k-\omega$ SST turbulence model since the transition model Gamma ReTheta only is compatible with the $k-\omega$ SST.

For all simulations the schemes for the convective and diffusive terms are 2nd-order. For the resistance and self-propulsion simulations, damping is applied on side and outlet boundaries to avoid wave reflections.

All simulations are conducted in calm water. The calm free surface in the resistance and self-propulsion simulations is resolved using the volume of fluid (VOF) method in STAR-CCM+ [14,19]. Hence, the volume fraction α is assigned and evolves in time with the following transport equation:

$$\frac{\partial \alpha}{\partial t} + \frac{\partial}{\partial x_i}(\alpha u_i) = 0 \tag{5}$$

The transport equation is solved using the High-Resolution Interface Capturing scheme [20]. The effective fluid properties are weighted using the volume fraction:

$$\rho = \alpha\rho_w + (1-\alpha)\rho_a \tag{6}$$

$$\mu = \alpha\mu_w + (1-\alpha)\mu_a \tag{7}$$

where ρ_w is the density of the water phase, ρ_a is the density of the air phase and μ_w and μ_a are the corresponding dynamic viscosities.

The solver for the temporal discretization is a first-order scheme, and the convective Courant number is kept below 1 in most of the domain. The heave and pitch motions of the vessel are solved using the Dynamic Fluid Body Interaction (DFBI) model in STAR-CCM+ cf. [14] and is applied as a rigid translation and rotation of the mesh.

The convergence of the simulations has been closely monitored by visual expectation for each simulation. This has been done to ensure that the changes to the solution and the running-means of the results are negligible at the end of the simulation.

The propeller thrust coefficient K_T is defined as:

$$K_T = \frac{T}{\rho_w n^2 D^4} \tag{8}$$

where n is the propeller rate of revolution in s^{-1} and D is the propeller diameter.

The propeller torque coefficient K_Q is defined as:

Table 2
Number of cells and required computational cost for a single simulation. OW is open-water. All simulations are performed on 16-core nodes (Xeon E5-2650 running at 2.60GHz)

Simulation	No. of cells	Comp. cost
Resistance	4.4M	3 hours on 112 cores
Propeller OW	7.5M	30 min on 112 cores
Self-propulsion	10.0M	2 days on 112 cores

$$K_Q = \frac{Q}{\rho_w n^2 D^5} \tag{9}$$

The propeller open-water efficiency η_o is defined as:

$$\eta_o = \frac{JK_T}{2\pi K_Q} \tag{10}$$

where $J = \frac{V_A}{nD}$ is the advance ratio, and V_A is the advance speed. The delivered power P is calculated as:

$$P = 2\pi n Q \tag{11}$$

3.2. Grid convergence index

For the verification study of each CFD set-up, the discretization error is estimated using the Grid Convergence Index (GCI) method [21] which is based on Richardson extrapolation, cf. [22,23]. The apparent order (p) is calculated by:

$$p = \frac{1}{\ln(r_{21})}|ln|\epsilon_{32}/\epsilon_{21}| + q(p)| \tag{12}$$

$$q(p) = \left(\frac{r_{21}^p - s}{r_{32}^p - s}\right) \tag{13}$$

$$s = \text{sgn}(\epsilon_{32}/\epsilon 21) \tag{14}$$

where r are refinement ratios, $\epsilon_{32} = \phi_3 - \phi_2$, $\epsilon_{21} = \phi_2 - \phi_1$, and ϕ_k denotes the solution on the k-th mesh. $q(p) = 0$ for $r = \text{const}$. The extrapolated asymptotic value is calculated as:

$$\phi_{ext}^{21} = \frac{r_{21}^p \phi_1 - \phi_2}{r_{21}^p - 1} \tag{15}$$

Different error estimates can now be calculated. The approximate relative error is:

$$e_a^{21} = \left|\frac{\phi_1 - \phi_2}{\phi_1}\right| \tag{16}$$

The extrapolated relative error is:

$$e_{ext}^{21} = \left|\frac{\phi_{ext}^{12} - \phi_1}{\phi_{ext}^{12}}\right| \tag{17}$$

The GCI for the fine and medium mesh is calculated as follows using the safety factor of 1.25 recommended by Roache [24]:

$$GCI_{\text{fine}}^{21} = \frac{1.25 e_a^{21}}{r_{21}^p - 1} \tag{18}$$

$$GCI_{\text{medium}}^{32} = \frac{1.25 e_a^{21} r_{21}^p}{r_{21}^p - 1} \tag{19}$$

The GCI value will be used to indicate the discretization error, since the GCI value is a measure of the discrepancy between the computed value and the asymptotic numerical value.

3.3. Modelling of roughness on the hull and propeller

In full-scale, the roughness on most areas of the hull and propeller cannot be assumed smooth. The effects of hull roughness are implemented using two different approaches. One approach is to estimate the roughness resistance using empirical formulas and apply it as a point force in the center of gravity. The first widely used correlation formula was proposed by Bowden and Davidson [25]:

$$\Delta C_{F,Bowden-Davidson} = \left[105\left(\frac{AHR}{L_{WL}}\right)^{\frac{1}{3}} - 0.64\right] \times 10^{-3} \tag{20}$$

where $\Delta C_{F,Bowden-Davidson}$ is the correlation factor and AHR is the average hull roughness. If there are no measured data, ITTC recommends using AHR = 150μm [26].

The Bowden-Davidson correlation formula both includes the effect of roughness and a general model-ship correlation. The formulae is based on thrust and roughness measurements on 14 ships. Hence, Bowden and Davidson [25] calculated the discrepancy between the sea trial measurements and the model tank prediction using six different form factor methods. For each form factor method, a fitted mean curve describing the relation between the discrepancy and the measured hull roughness was found based on the 14 measurements. A final correlation was found as the mean of the six mean curves was found. The relation for this final mean curve is the relation shown in Eq. 20. Townsin and Mosaad [27] proposed the following new empirical relation which only include the effect of roughness:

$$\Delta C_{F,Townsin} = 0.044\left[\left(\frac{\text{AHR}}{L_{WL}}\right)^{\frac{1}{3}} - 10 \times \text{Re}^{-\frac{1}{3}}\right] + 0.000125 \tag{21}$$

The correlation factor (C_A) accounts for everything not included in the extrapolation procedure, e.g. 3D-effects and scaling effects. The Townsin formulas ($\Delta C_{F,\ Townsin}$ and C_A) replaced the Bowden-Davidson formula in the ITTC-recommended procedure in 2008. The definition of C_A as formulated by ITTC [26] is:

$$C_A = (5.68 - 0.6\log(\text{Re})) \times 10^{-3} \tag{22}$$

It should be noted that based on a questionnaire by ITTC [28], almost no towing tanks are using the ITTC standard C_A-value (Eq. 22). Instead towing tanks are mainly using their own C_A formula or the older Bowden-Davidson formula (Eq. 20).

In the CFD simulations where the roughness resistance is empirically estimated, Eq. 21 will be used with the recommended roughness height of 150μm. A correlation allowance C_A will not be used since the CFD simulations will be conducted in full-scale. The roughness resistance from the empirical formula is added to the ship resistance in the force balance as a concentrated point force. Propeller roughness is not considered when using the empirical formula.

An alternative method is to model the effects of roughness in the CFD calculation by applying a roughness function and modify the wall functions as proposed by Cebeci and Bradshaw [9]. In the logarithmic region of the turbulent boundary layer, the mean velocity profile for a smooth surface is described as:

$$U^+ = \frac{1}{\kappa}\ln y^+ + B \tag{23}$$

where $U^+ = \frac{U}{U_\tau}$ is the non-dimensional velocity in the boundary layer, κ is the von Karman constant equal to 0.42, $y^+ = \frac{yU_\tau}{\nu}$ is the non-dimensional normal distance to the wall, ν is the kinematic viscosity, $U_\tau = \sqrt{\tau_w/\rho}$ is the friction velocity, τ_w is the shear stress at the wall and B is smooth wall log-law intercept.

The roughness elements on the surface increase the turbulence in the boundary layer. Clauser [29] showed that the effects of surface roughness results in a downwards shift in the velocity profile. This downward shift is termed a "roughness function". Hence, for a rough surface, the mean velocity profile can be described as:

$$U^+ = \frac{1}{\kappa}\ln y^+ + B - \Delta U^+ \tag{24}$$

where ΔU^+ is the roughness function. There is no universal roughness function. Normally the roughness function is determined experimentally for a given flow over a rough surface. The roughness function can be expressed as a function of the roughness Reynolds number R_s^+, which is defined as:

$$R_s^+ = \frac{R_s U_\tau}{\nu} \tag{25}$$

where R_s is the equivalent sand-grain roughness height. The roughness

function used in the present study is proposed by Demirel et al. [30], based on the experiments by Schultz and Flack [31], and can be expressed as:

$$\Delta U^+ = \begin{cases} 0, & \text{if } R_s^+ < 3. \\ \frac{1}{\kappa}\ln(0.26R_s^+)\sin\left[\frac{\pi}{2}\frac{\log(R_s^+/3)}{\log(5)}\right], & \text{if } 3 < R_s^+ < 15. \\ \frac{1}{\kappa}\ln(0.26R_s^+), & \text{if } R_s^+ > 15. \end{cases} \quad (26)$$

A well-known problem with surface roughness is the difficulty to describe the roughness parameters such as height, density and shape of the roughness elements as one parameter, cf. [32]. Furthermore the height, density and shape of the roughness elements often vary across the surface.

Unlike describing the roughness height as the mean roughness height R_a, root-mean-square R_{rms} or maximum peak-to-through height R_t, the equivalent sand-grain roughness height R_s, which is also denoted k_s, [33] cannot be directly measured on the surface. Instead, R_s describes the influence of the surface roughness on the wall-bounded flow and can be found experimentally using a Moody diagram or from literature values.

Lindholdt et al. [34] present an extensive literature study on biofouling on ships and experimental methods used to quantify the drag penalty of the hull coating. They conclude that knowledge about the relation between surface roughness and hydrodynamic drag is very limited. However, the drag penalty from hard macro-fouling is better understood than soft biofouling.

In the present study, the vessels are newly cleaned and painted and hard macro-fouling is unlikely. If some areas of the ship hull get fouling from the time between launch and speed trial, the expected type of biofouling type will be soft. The fouling is especially expected in the vessel side facing the sun and the area near the free surface.

Unfortunately, the exact roughness of the vessel and propeller is unknown. This includes the height, shape, skewness and kurtosis of the roughness elements as well as the density and distribution of these on the hull and propeller. Since this is unknown, a literature study on the measured roughness of newly painted ships is conducted.

Utama et al. [35] measured the surface roughness on a newly painted ship hull using a silicone rubber surface imprint. The results of the scanning of the imprint can be seen in Table 3. These roughness measurements were a factor of two to three higher than the measurement by Schultz [36], who measured the roughness of different paint types on plates. For the two silicone paints, the roughness heights are shown in Table 3. This significant difference between roughness height on a painted ship and a painted plate could indicate that the paint roughness is highly dependent on the way the paint is applied. A study by Niebles Atencio and Chernoray [37] who painted three plates with the same paint but with different paint application quality supports this. As seen in Table 3, the quality of the paint application has a significant influence on the paint roughness height with a factor of up to ten.

Schultz et al. [38] have conducted a study where three plates were painted with different anti-fouling paints. The plates were exposed to an environment similar to a ship hull. The roughness height was measured before the exposure and after three and six months of exposure and a mean roughness height up to 574μm was measured. The results are shown in Table 3, and the roughness heights were for the areas covered by biofouling. The surface coverage of biofilm was between 6.4% − 48.2%.

A study by Usta and Korkut [39] measured five plates painted with anti-fouling paint. The surface properties were measured using four different measuring lengths also called "cut-off" in the range from 0.008mm − 2.5mm. Only the measurements from the 2.5mm are shown in Table 3 since most of the other studies have a cut-off of up to 50mm. Usta and Korkut [39] found that the length of the cut-off has an influence on the measured roughness heights with a factor of up to two. The conclusion is similar to the study by Howell and Behrends [40], who compared surface roughness measurements of anti-fouling coatings from different studies where the cut-off length is available. Howell and Behrends [40] found that the factor can be even larger than two.

It is not only on the ship hull that surface roughness affects the performance of the vessel. The propeller is also a non-smooth surface where fouling occurs in operation. A CFD study by Owen et al. [41] showed that roughness significantly decreases the efficiency of the propeller. The influence of roughness on the propeller performance explains why propeller polishing has been a widely used treatment for many years.

Based on this literature study it is found that the peak-to-though height R_t for a newly painted plate or ship is in the range of 2.2μm − 479.1μm. This range is very wide due to the differenct types of paint, quality of application and potential underlying imperfections from previous paintings etc.. It is important to mention that the $R_t = 479.1\mu$m by Utama et al. [35] is a measurement on a real ship. The other roughness measurements are performed on painted flat plates in the laboratory. The measurements by Utama et al. [35] are conducted in the dry dock before the launch. From the time the newly painted ship is launched, the ship is moored several months at the quayside for outfitting. During these months, slime starts to develop on the hull increasing the hull roughness. Especially in the areas near the free surface at the side facing away from the quay. When transforming the measurable R_t to non-measurable R_s, unfortunately no universal relation is available. The study by Adams et al. [42] showed that R_t is approximately equal to R_s if the surface roughness is a monolayer of closely packed spheres of uniform diameter. The relations are shown in Table 4. Schultz [43] found that the relation between R_t and R_s is dependent on the roughness height. For a newly applied paint, Schultz [43] found that the R_t is approximately five times larger than R_S. For very rough surfaces, R_t and R_s become equal, cf. Schultz [43]. Since the actual roughness of the vessels on the day of the speed trial is not available, CFD simulations are conducted using a range of roughness heights. Based on the literature described above, the chosen roughness heights used in the CFD simulations presented in Sec. 4.3 are $R_s = 100\mu$m, $R_s = 120\mu$m and $R_s = 150\mu$m.The roughness of the propeller is set to $R_s = 30\mu$m for all simulations presented in Sec. 4.3.

Table 3
Comparison of measured roughness heights from various studies. R_a is the mean roughness height, R_{rms} is the root-mean-square, and R_t is the maximum peak-to-through height.

Study	Comment	$R_a[\mu m]$	$R_{rms}[\mu m]$	$R_t[\mu m]$
[35]	Newly painted ship	41.3	51.9	479.1
[36]	Painted plates	10 − 19	13 − 23	66 − 142
[37]	Optimal airless application		8.5	56
	Poor application		41	214
	Very poor application		85	420
[38]	Clean painted plate	0.4 − 1.0	0.5 − 1.2	2.2 − 4.7
	After 3 months exposure	443 − 574		
	After 6 months exposure	98 − 520		
[39]	Painted plates	1.8 − 4.5	2.1 − 5.2	8.4 − 18.6

Table 4
Estimated relation between measured roughness height and equivalent sand-grain roughness height. R_a is the mean roughness height, R_{rms} is the root-mean-square, R_t is the maximum peak-to-through height and R_s is the equivalent sand-grain roughness height [42].

Roughness parameter	Estimated R_s
R_a	$R_s = 5.863R_a$
R_{rms}	$R_s = 3.1R_{rms}$
R_t	$R_s = 0.978R_t$

3.4. Validation and convergence test

It is of uppermost importance to ensure the accuracy of the CFD set-up before conclusions are based on the results of the set-up. In this study, both convergence studies for verification and comparison studies for validation are performed for each CFD set-up. The most important of the convergence studies and comparison studies for the ro-ro vessel are presented in the following sections.

3.4.1. CFD resistance

All resistance simulations are performed in the speed trial condition, as described in Sec. 2.1, similar to the towing tank tests and speed trials. Both the rudders and shafts are included. The initial CFD set-up used to estimate the calm water resistance is an automated CFD set-up originally developed by OSK-ShipTech A/S. The set-up has been developed further in the present study.

In the CFD resistance set-up a number of different physics models are used to model the flow around the ship. Free surface waves are modelled using VOF, as described in Sec. 3.1. The hull is allowed dynamic pitch and heave motions. The simulations are solved using a first-order implicit unsteady solver.

The shape of the domain is a rectangular box. Only one half of the twin screw ro-ro vessel is modelled since the flow is considered to be symmetrical. A test simulation with a larger domain is conducted to ensure that the domain is significantly large to not affect the results. The domain can be seen in Fig. 2 and the boundary conditions can be seen in Table 5. The top and bottom boundaries are inlets, since fluid will flow through these when the pitch is non-zero. The volume mesh consists of hexahedrons in a unstructured grid. The mesh is generated using the trimmer-mesh function in STAR-CCM+. The boundary layer mesh, also called the prism layer mesh, is used on the hull surface in order to ensure accurate estimation of the wall shear stress within the wall function approximation. Fifteen prism layers are used on the ship hull and appendages. The wall y^+ values on the hull are mostly in the range of 50–200. The mesh is refined in the important zones including the free surface, transom, bulbous bow etc.. The mesh on the free surface can be seen in Fig. 3. The full-scale resistance set-up is created by scaling up the model scale resistance set-up with the scaling factor. The boundary layer is changed so the wall y^+ is still mostly in the range of 50–200. The air resistance is calculated using the standard ITTC method, [26], with the recommended drag coefficient of 0.8 and is added to the ship resistance. The magnitude of the air resistance is approximately 5 percent of the total resistance. The drag from the bow thrusters is estimated using the method proposed by ITTC [26] and is added to the ship resistance. The magnitude of the bow thruster drag is approximately 1 percent of the total resistance.

For all resistance simulations, the empirical formula from Townsin (Eq. 21) is used to estimate the roughness resistance which is applied as a point force in the center of gravity. the propeller open-water test using CFD is less complex than modelling the self-propulsion test because the hull-propeller interaction is not included in the propeller open-water set-up.

The single phase propeller open-water set-up uses two domains: a stationary domain and a rotating domain. The two domains are connected by an interface. The shape of the stationary domain is a rectangular cubeoid. The shape of the rotating domain is a cylinder which is located inside the static domain and around the propeller. The size of the rotating domain is the same as in the self-propulsion simulation. An illustration of the domains can be seen in Fig. 4 and boundary conditions of the domains are listed in Table 6. The volume mesh in the stationary domain consists of hexahedrons in an unstructured grid. In the rotating domain, the mesh is polyhedral due to the complex propeller geometry. Fifteen prism layers are used on the shaft, blades and hub. In order to better resolve the flow around the propeller, two refinement zones are used to refine the mesh in the volume around the

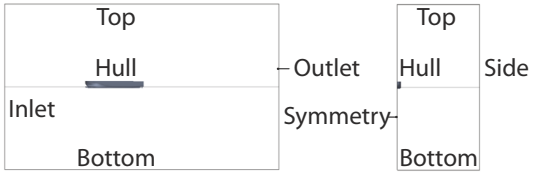

Fig. 2. Domain of the resistance set-up and self-propulsion, with boundary names. Thin line is the free surface. Seen from starboard side (left) and from the front (right).

Table 5
Boundary conditions of the CFD resistance set-up.

Name of boundary	Boundary condition
Inlet	Velocity inlet
Top	Velocity inlet
Bottom	Velocity inlet
Outlet	Pressure outlet
Symmetry	Symmetry plane
Side	Slip wall
Hull	No-slip wall

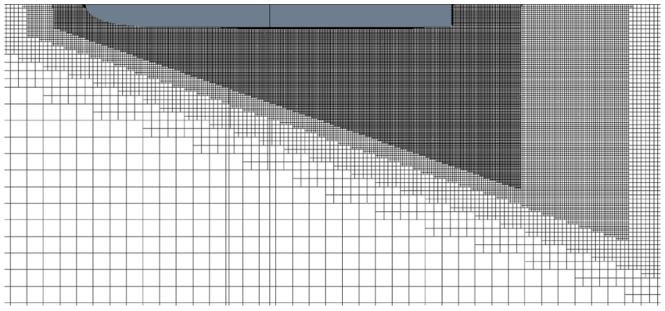

Fig. 3. Close-up of mesh on the free surface for resistance simulation seen from top.

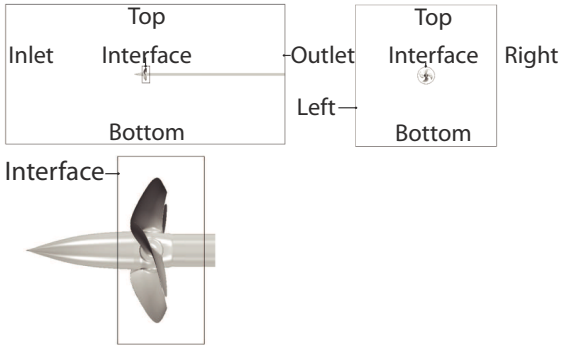

Fig. 4. Domain of the CFD propeller open-water set-up for the ro-ro vessel, with boundary names. Seen from the side (upper left and bottom) and from the front (upper right).

Table 6
Boundary conditions of the CFD propeller open-water set-up.

Name of boundary	Boundary condition
Inlet	Velocity inlet
Outlet	Pressure outlet
Top	Symmetry plane
Bottom	Symmetry plane
Left	Symmetry plane
Right	Symmetry plane
Interface	Internal interface
Shaft, Blades, Hub	No-slip wall

propeller. In model scale, the rotation rate and advance speed of the propeller in the CFD simulation are equal to the rate of rotation and advance speed used in the towing tank. In full-scale, the rotation rate and advance speed of the propeller is set similar to what the actual ship will experience. The propeller movement can be modelled using two different methods: the moving reference frame method (MRF) or the sliding mesh (SM).

The MRF method works by changing the reference system from a stationary coordinate system to a rotating coordinate system moving with a constant rotational velocity. This is also called a ”frozen rotor” approach. SM works by rotating the propeller geometry and surrounding cylindrical mesh region in increments at each new time step. The rotational cylindrical mesh region has a sliding interface to the surrounding stationary mesh. This method requires more computational time, but is a better model of the actual propeller physics compared to the MRF method. The SM method models the hull-propeller interaction while the MRF method does not. Since there is no hull in the propeller open-water simulations, the MRF method is used.

In model scale, the Gamma ReTheta transition model (see Sec. 3.1) is used to estimate the laminar to turbulent transition on the propeller. In full-scale, the transition model is not used since the flow is assumed fully turbulent due to the high Reynolds number. On the inlet boundary condition, the turbulence intensity is set to 1%, and the turbulent viscosity ratio is set to one.

The propeller open-water CFD set-up uses wall functions, and the y + values on the propeller are mostly in the range of 100–250 in the full-scale simulations. In model scale the y+ values on the propeller are mostly below one, which is required when using the transition model.

3.4.2. CFD self-propulsion

The self-propulsion set-up is created by combining the verified and validated resistance CFD set-up with the verified and validated propeller open-water CFD set-up. As in the propeller open-water set-up, the domain consists of two domains. The mesh in the stationary domain consists of hexahedrons in an unstructured grid. In the rotating domain, the mesh is polyhedral cells. Using two separate meshes allows mesh settings from the resistance set-up to be used for the static domain and mesh options from the propeller open-water set-up to be used for the rotating domain. The static domain can be seen in Fig. 2. Isotropic mesh refinement zones are used in the self-propulsion set-up to better resolve the flow between the hull and propeller. The mesh near the aft ship can be seen in Fig. 5. The boundary conditions of the domains can be seen in Table 7. The rotating domain and the interface can be seen in Fig. 5 where the mesh is polyhedral. All self-propulsion simulations are conducted in speed trial condition, and only half of the twin screw ship is simulated since the flow is considered symmetric. The resolved flow around the propeller is illustrated in Fig. 6.

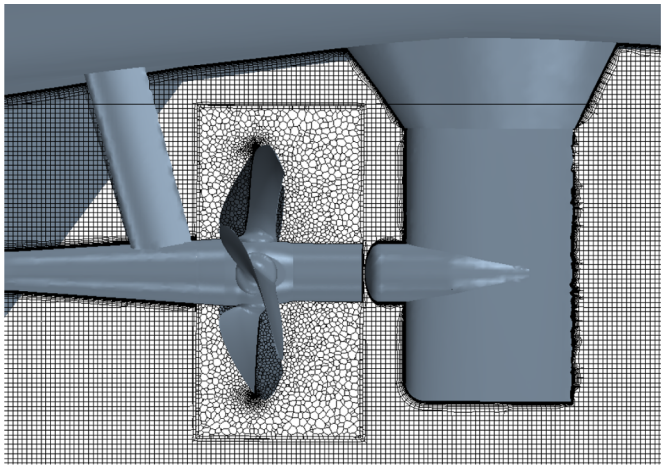

Fig. 5. Side view of self-propulsion mesh in shaft plane of the ro-ro vessel.

Table 7
Boundary conditions of the CFD self-propulsion set-up.

Name of boundary	Boundary condition
Inlet	Velocity inlet
Bottom	Velocity inlet
Outlet	Pressure outlet
Top	Velocity inlet
Symmetry	Symmetry plane
Port Side	Slip wall
Interface	Internal interface
Hull and propeller	No-slip wall

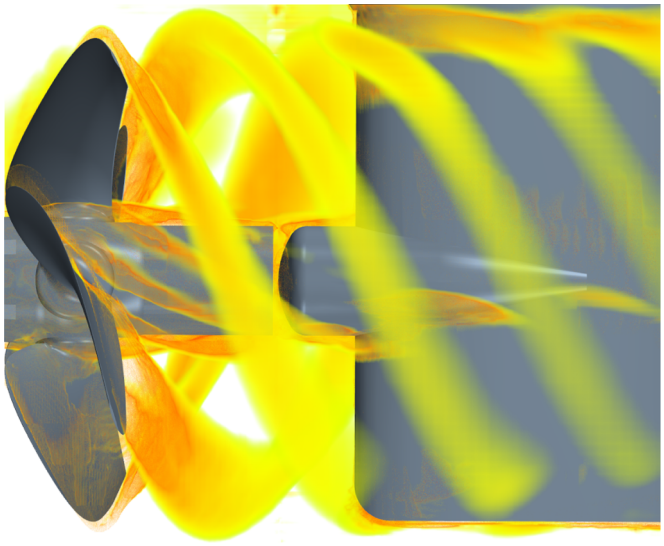

Fig. 6. Vorticity downstream of the ro-ro vessel propeller in a self-propulsion simulation.

As in the resistance CFD set-up, the free surface is resolved using the VOF method. An illustration of the wave elevation in a self-propulsion simulation is shown in Fig. 7.

The dynamic pitch and heave are calculated in a separate simple self-propulsion simulation where the propeller is modelled using an actuator disc, and the hull and propeller are free to heave and pitch. The actuator disc is a simplified axis-symmetric model of the propeller. The actuator disc accelerates the flow over the disc area based in the propeller open-water characteristics. The presence of the actuator disc creates a pressure distribution in the aft ship required to accurately estimate the dynamic heave and pitch. The thrust from the actuator disc is added as a concentrated force on the shaft. The dynamic pitch and heave from this simplified self-propulsion simulation are used as fixed in the self-propulsion simulation with the geometrically rotating propeller. The self-propulsion simulation using the actuator disc only requires a fraction of the computational cost of the self-propulsion simulation with the sliding mesh approach.

For the self-propulsion simulations a combination of transient MRF and SM is used for increased computational efficiency. For 200 physical seconds, corresponding to approximately 400 propeller revolutions, the propeller is modelled using MRF to efficiently develop the flow around the ship and free surface. For the first 100 seconds, the time step is equal to the time step used for the resistance simulations. For the next 100 seconds a finer time step is used. After 200 seconds of using the MRF approach, the SM approach is used for the remaining part of the simulation. The SM uses a time step corresponding to two degrees of propeller rotation.

The rate of revolution of the propeller is changed using a p-controller until a force balance is obtained in the sailing direction within

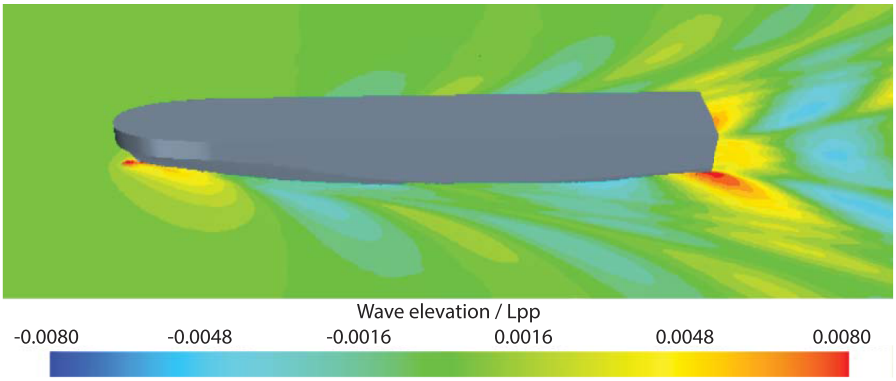

Fig. 7. Wave elevation from full-scale self-propulsion simulation of the ro-ro vessel in speed trial condition at Fn = 0.268

0.5%, which is half the 1% tolerance recommended by ITTC [44]. The force balance is taken in the direction parallel to the shaft axis. The drag from the bow thruster and wind loads is also included in the force balance.

The model scale CFD self-propulsion set-up is carried out using the same principle with the exact same tow rope force as used by the towing tank. The full-scale self-propulsion set-up is created by scaling up the model scale self-propulsion set-up according to the scaling factor. The prism layers are changed so the wall y^+ is mostly in the range of 30–200 on the hull and propeller. The force balance in full-scale is slightly different from model scale since the effect from air resistance and roughness on the hull and propeller is included. The two different approaches of including the roughness on the hull and propeller are explained in Sec. 3.3.

For the self-propulsion simulations using the Townsin roughness allowance (Eq. 21), the force balance is including the total drag on the ship, the propeller thrust, the empirically estimated wind and bow thruster resistance and the empirically estimated roughness resistance. The results of these simulations can be seen in Sec. 4.2. The total drag is found by integrating the pressure and shear distribution on all ship surfaces besides the propeller. When roughness is included using modified wall functions, the force balance only includes the total drag on the ship, the propeller thrust and the empirically estimated wind resistance and the bow thruster drag. The results of these simulations are shown in Sec. 4.3.

All power results for the ro-ro vessel are presented as delivered power as a percentage of Maximum Continuous Rating (MCR). Therefore, the loss in gears and shaft bearings are not included. This is considered reasonable, since the power is measured aft of the gear during the speed trial.

4. Results and discussion

In the following sections, the results of the speed trial measurements for the ro-ro vessel will be presented followed by a comparison with the towing tank prediction. Afterwards the CFD set-ups will be verified and validated, and finally the full-scale self-propulsion CFD results will be compared with the speed trial results. Only Sec. 4.3.1 presents results on the general cargo vessel. All other sections present results of the ro-ro vessel.

4.1. Speed trial measurements and comparison with towing tank prediction

The speed trial results provided by the shipyard are the measured values corrected for wind and current. The procedures of the speed trial and corrections are briefly described in Sec. 2.4. The results of the corrected delivered power as function of Froude number from the speed trials of the six sister vessels are shown in Fig. 8. It is challenging to choose a regression type to fit the results to a mean curve. The obvious

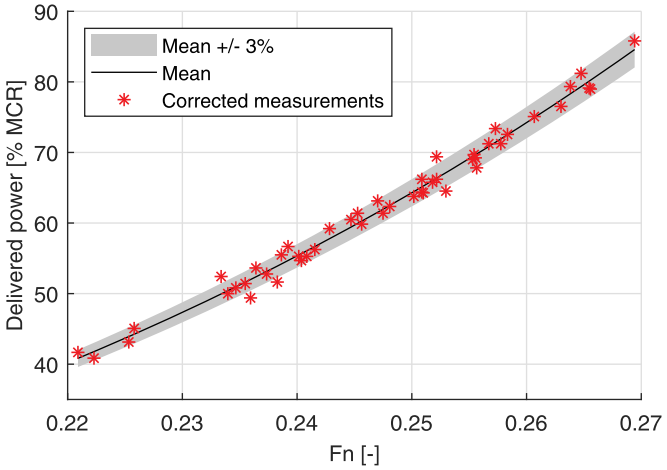

Fig. 8. Corrected speed trial measurement for the six ro-ro vessels including mean curve.

choice would be a power regression of the form $P_d = a\mathrm{Fn}^b$ where a and b are constants and P_D is the delivered power in percentage of MCR. In classical fluid mechanics, the power is proportional with the speed to power of three. However, for ship resistance b is not constant and mostly higher than three. Without the consideration of humps and hollows, b is increasing when the ship speed is increasing, due to the wave generation. However, in this study, a and b are considered constant in the limited speed range. The fitted mean curve valid for the speed range $\mathrm{Fn} = 0.22 - 0.27$ is found to be $P_D = 0.228\mathrm{Fn}^{3.560}$. The R^2-value of the fit is 0.9981. Most of the corrected speed trial measurements are within 3% of the mean curve, as seen in Fig. 8. It is very satisfactory with such a low scatter of the data points considering construction tolerances and measurements uncertainties when building and testing six 200m sister vessels. This indicates that the accuracy of the speed trial data is high and therefore a good reference for the validation study.

In order to validate the three different CFD set-ups in both model and full-scale in systematic steps, a more detailed set of accurate data is required. A full set of towing tank measurements and predictions is a good data set for this purpose. More details on the towing tank testing are found in Sec. 2.3. However, before these data are used, the full-scale towing tank prediction is compared with the mean speed trial curve. The discrepancy is within 1 percent for all speeds as seen in Table 8. This is considered very good and within the uncertainty of both the prediction and the speed trials. It should be noted that HSVA have used their own confidential correction formula for roughness and not the one recommended by ITTC. This excellent agreement indicates that the towing tank measurements and predictions are a good data set for validating the different CFD set-ups.

Table 8
Discrepancy of ro-ro vessel full-scale self-propulsion results from speed trial compared to towing tank prediction.

Froude number	Delivered power
0.222	− 0.9%
0.245	0.1%
0.268	0.5%

4.2. CFD with emperical roughness

The following sections present the validation and results of the resistance, propeller open-water and self-propulsion CFD simulations. All results in Sec. 4.2 have been submitted to the shipyard without knowing the towing tank measurement and predictions and sea trial results. After the submission of the CFD results, the shipyard shared the full towing tank report with the authors. In this section, the hull roughness is estimated using the empirical Townsin formula (Eq. 21) and applied in the center of gravity as discussed in Sec. 3.3. Roughness on the propeller is not considered in this section.

4.2.1. Verification and validation of the resistance simulations

The mesh convergence study of the resistance set-up, described in Sec. 3.4.1, is conducted at the lowest Froude number, because a lower Froude number gives shorter distance between the generated waves. The shorter the distance is, the finer mesh is required. Conversely, the time step convergence study is conducted at the highest Froude number since simulations at higher speeds have the highest Courant number. The spatial and temporal discretization error is estimated using the GCI method described in Sec. 3.2. The summery is presented in Table 9. It can be seen that the spatial and temporal GCIs for the medium mesh is 1.3% and 0.3% respectively. Both are within the uncertainty of the model test experiments and are therefore considered acceptable. Resistance simulations are conducted using the medium mesh and medium time step and the total resistance coefficients are compared with extrapolated towing tank results in Table 10. The comparison with extrapolated towing tanks results shows good agreement with underestimation in total resistance in CFD of up to 2.5% compared to towing tank extrapolation.

4.2.2. Verification and validation of propeller open-water simulations

The result of the convergence study of the model scale propeller open-water CFD set-up shown in Table 11. It is seen that the spatial GCIs for thrust, torque and efficiency are lower than 2.5% for the medium mesh. It is therefore decided to use the medium mesh in the comparison studies. The exact uncertainty from the propeller open-water towing tank test is unknown. However, the difference between the measured propeller open-water characteristics in the towing tank report of the port and starboard propeller was up to 4%. It is known that exact pitch setting of the model scale propeller is subject to some uncertainty. To study the sensitivity of pitch setting, a sensitivity study is conducted and it is found that 1 degree of pitch changes the thrust and torque with up to 15% and the efficiency with up to 4%. For both model and full-scale, the model scale propeller open-water CFD results are compared with the measured towing tank results in Table 12. The discrepancy in the propeller open-water characteristics between towing tank measurements and CFD is less than 5.5% for the advance ratio of approximately 0.86 where the propeller is operating. At the lower advance ratio where the propeller is normally not operating thrust and torque are overestimated with up to 10.1% and efficiency with up to 3.5%.

The results for the full-scale mesh convergence study show that the spatial GCIs for thrust, torque and efficiency are lower than 1.0% for the medium mesh, cf. Table 13. It is therefore decided to use the medium mesh. When comparing the full-scale propeller open-water CFD results with the towing tank predictions, as shown in Table 14, is is seen that the discrepancy in the propeller open-water efficiency is less than 1% for the advance ratio of approximately 0.86 where the propeller is operating. The thrust and torque are overestimated with up to 6.3% at these advance ratios. At the lower advance ratio where the propeller is normally not operating, thrust and torque are overestimated with up to 7.9%, and the propeller open-water efficiency is overestimated with up to 1.2%.

Table 9
Estimation of spatial and temporal discretization error in total resistance coefficient for full-scale resistance simulations of the ro-ro vessel.

	Spatial	Temporal
r_{21}	1.49	2
r_{32}	1.55	2
ϕ_1	0.002056	0.002723
ϕ_2	0.002074	0.002718
ϕ_3	0.002224	0.002698
p	4.73	1.9
ϕ_{ext}^{21}	0.002053	0.002725
e_a^{21}	0.889%	0.194%
e_{ext}^{21}	0.158%	0.071%
GCI_{fine}^{21}	0.197%	0.089%
GCI_{medium}^{32}	1.309%	0.330%

Table 10
Discrepancy of ro-ro vessel full-scale total resistance from CFD compared to towing tank prediction.

Froude number	Total resistance
0.222	− 2.5%
0.245	− 1.9%
0.268	− 1.5%

Table 11
Estimation of spatial discretization error for model scale propeller open-water simulation of the ro-ro vessel.

	KT	KQ	ETA_0
r_{21}	1.33	1.33	1.33
r_{32}	1.35	1.35	1.35
ϕ_1	0.3090	0.0512	0.5769
ϕ_2	0.3073	0.0510	0.5749
ϕ_3	0.3047	0.0509	0.5717
p	1.1994	0.8036	1.4485
ϕ_{ext}^{21}	0.3131	0.0516	0.5806
e_a^{21}	0.555%	0.218%	0.337%
e_{ext}^{21}	1.324%	0.828%	0.647%
GCI_{fine}^{21}	1.677%	1.044%	0.813%
GCI_{medium}^{32}	2.370%	1.316%	1.235%

4.2.3. Verification and validation of self-propulsion simulations

The medium mesh and time step at the self-propulsion CFD set-up

Table 12
Discrepancy of ro-ro vessel model scale propeller open-water characteristics from CFD compared to towing tank prediction.

Advance ratio	Thrust coefficient	Torque coefficient	Open-water efficiency
0.5	10.1%	8.5%	1.4%
0.6	9.7%	6.8%	2.7%
0.7	8.3%	4.6%	3.5%
0.8	5.4%	2.1%	3.3%
0.9	3.7%	0.9%	2.8%
1.0	2.6%	− 0.4%	3.0%

Table 13
Estimation of spatial discretization error for full-scale propeller open-water simulation of the ro-ro vessel.

	KT	KQ	ETA_0
r_{21}	1.4687	1.4687	1.4687
r_{32}	1.3214	1.3214	1.3214
ϕ_1	0.3269	0.0552	0.5656
ϕ_2	0.3255	0.0551	0.5637
ϕ_3	0.3237	0.0552	0.5605
p	1.9227	4.2094	2.6369
ϕ_{ext}^{21}	0.3281	0.0552	0.5667
e_a^{21}	0.413%	0.078%	0.336%
e_{ext}^{21}	0.376%	0.019%	0.191%
GCI_{fine}^{21}	0.472%	0.024%	0.239%
GCI_{medium}^{32}	0.988%	0.121%	0.658%

Table 14
Discrepancy of ro-ro vessel full-scale propeller open-water characteristics from CFD compared to towing tank prediction.

Advance ratio	Thrust coefficient	Torque coefficient	Open-water efficiency
0.5	7.8%	7.1%	0.6%
0.6	7.9%	6.8%	1.0%
0.7	7.4%	6.2%	1.2%
0.8	6.3%	5.5%	0.8%
0.9	5.3%	5.2%	0.1%
1.0	5.3%	5.3%	− 0.1%

Table 15
Estimation of spatial and temporal discretization error in delivered power for model scale self-propulsion simulations of the ro-ro vessel.

	Spatial	Temporal
r_{21}	1.1613	1.5000
r_{32}	1.2070	2.0000
ϕ_1	112.7	107.8
ϕ_2	113.1	107.2
ϕ_3	113.4	106.8
p	3.6029	4.3142
ϕ_{ext}^{21}	112.1	107.9
e_a^{21}	0.342%	0.544%
e_{ext}^{21}	0.481%	0.114%
GCI_{fine}^{21}	0.599%	0.143%
GCI_{medium}^{32}	1.026%	0.824%

Table 16
Discrepancy of ro-ro vessel model scale self-propulsion results from CFD compared to towing tank measurements.

Froude number	Mean thrust	Mean torque	Propeller RPM	Delivered power
0.222	0.4%	− 0.8%	− 1.6%	− 2.4%
0.245	− 1.3%	− 0.1%	− 1.5%	− 1.6%
0.268	− 3.2%	0.0%	− 1.5%	− 1.5%

corresponds to the medium mesh and time step from the resistance CFD set-up and propeller open-water CFD set-up. Table 15 shows that the spatial and temporal GCI for delivered power for model scale self-propulsion simulations each is approximately 1% for the medium mesh and time step, which is acceptable. Therefore, it is decided to use the medium mesh and medium time step corresponding to two degrees of propeller rotation in the following calculation. The self-propulsion CFD results in model scale have been compared with the towing tank measurements and a very good agreement is found. A general underestimation is observed with a maximum discrepancy of 3.2% for both thrust, torque, RPM and delivered power as presented in Table 16. The achieved advance ratio for the three self-propulsion points is approximately 0.86.

Table 17
Estimation of spatial and temporal discretization error in delivered power for full-scale self-propulsion simulations of the ro-ro vessel.

	Spatial	Temporal
r_{21}	1.306	2.000
r_{32}	1.411	2.000
ϕ_1	26.239	25.438
ϕ_2	25.802	25.390
ϕ_3	32.256	25.039
p	7.9549	2.88
ϕ_{ext}^{21}	26.299	25.445
e_a^{21}	1.668%	0.188%
e_{ext}^{21}	0.226%	0.030%
GCI_{fine}^{21}	0.283%	0.037%
GCI_{medium}^{32}	2.369%	0.272%

Mesh and time step convergence studies have also been conducted in full-scale as seen in Table 17. The temporal CGI is 0.3% when using the medium time step corresponding to two degrees or propeller rotation. For the medium mesh the spatial CGI is 2.4%. As shown in Table 2, each self-propulsion simulation takes approximately two days on 112 cores using the medium mesh. For the fine mesh the spatial GCI is 0.3%, but the required computational effort is impractically large for this study. Therefore, is has been decided to use the medium mesh and medium time step corresponding to two degrees of propeller rotation for the full-scale self-propulsion simulations.

The comparison between the full-scale CFD simulations and the towing tank prediction is shown in Table 18. As seen all parameters are significantly underestimated when using the traditional approach with the roughness allowance by Townsin (Eq. 21). This is surprising since the agreement between CFD and model tank for the previous simulations including full-scale resistance and model scale self-propulsion has been good. There are multiple contributors to the observed discrepancy. In terms of modelling errors, the use of realisable $k-\varepsilon$ RANS turbulence modelling can influence the results. A turbulence model sensitivity study is conducted by changing the turbulence model to $k-\omega$ SST. This changed the power with 2.7% (not shown). Modelling the wind resistance using the ITTC recommended procedure is another source of error. However, since the wind resistance account for less than 7% of the total resistance, any uncertainty of the wind resistance will only have a marginal effect on the estimated power. The temporal and spatial discretization error is also present and is attempted quantified in the GCI study to 2.4% and 0.3% respectively. Furthermore, the "to-be-built" hull and propeller geometry used in the CFD simulations are not identical to real ship. Lastly, the sea trial measurements do also have uncertainties. However, the sea trial results from the six sister vessels presented in Fig. 8 showed that by using the mean of these the contribution from building tolerances and sea trial measurements becomes small. So none of these contributes can explain the large discrepancies in full-scale.

4.3. Inclusion of roughness using wall functions

If the surface roughness of the hull and propeller is included in the

Table 18
Discrepancy of ro-ro vessel full-scale self-propulsion results from CFD compared towing tank prediction.

Froude number	Mean thrust	Mean torque	Propeller RPM	Delivered power
0.222	− 2.9%	− 6.6%	− 6.1%	− 12.2%
0.245	− 4.4%	− 5.5%	− 5.9%	− 11.1%
0.268	− 4.1%	− 3.1%	− 5.5%	− 8.4%

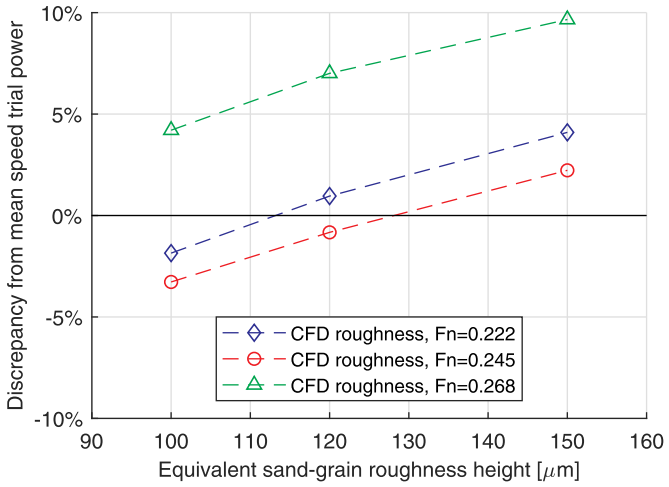

Fig. 9. Discrepancy of the ro-ro vessel CFD results compared to delivered power from speed trials as function of hull roughness height.

CFD simulation by modifying the wall functions, as described in Sec. 3.4.2, the discrepancy is significantly reduced, cf. Fig. 9. For the two lowest speeds the discrepancies between the delivered power from CFD and mean speed trial curve are within 4% for equivalent sand grain roughness heights between 100μm–150μm. These discrepancies are significantly smaller than the up to 12.2% found when using the Townsin roughness allowance. For the Froude number equal to 0.268, the delivered power is overestimated by 4.2% when R_s = 100μm and by 9.6% when R_s = 150μm. The discrepancies for the two lowest speeds are very similar, but the discrepancies for the larger speed is higher. This speed dependence is also seen in Table 18, where there is almost 3% difference in the delivered power discrepancy between Fn = 0.245 and Fn = 0.268. The reason for this gap is due to the unwanted flow around the aft part of the ship as shown in Fig. 10b. Fig. 10b shows that the flow is much worse seen from a hydrodynamic point of view compared to the flow in model scale as shown in Fig. 10a. When comparing the wave elevation at the aft part in a model scale self-propulsion simulation (not shown) and a full scale resistance simulation (not shown), it is seen that the the wave elevation is very similar. This is as expected when having identical Froude number. However, in full-scale self-propulsion the propeller is rotating at a much higher Reynolds number affecting the flow field near the propeller. At the lower speeds Fn = 0.222 and Fn = 0.245, is flow is much smoother (not shown). This is believed to be the reason for the significant speed dependence at the highest speed (Fn = 0.268) in full scale cf. Table 18 and Fig. 9 and not in model scale cf. Table 16. This shows that the influence of the propeller Reynolds number can affect the wave elevation near the aft, if the water line comes close to the propeller. This is the case at the very light sea trial condition. It is important to note that the ship is not likely to sail at such a light condition at this very high speed other than at the sea trial. The R_s^+ is approximately 10–60 on both the hull and propeller as seen in Figs. 11 and 12. Thus, the R_s^+ is smaller than the wall $y+$ in all cells. This is done in order to avoid under-prediction of the frictional resistance as discussed by Eca and Hoekstra [45].

These results indicate that modelling of the roughness using modified wall functions can significantly improve the accuracy of the full-scale CFD prediction compared to the traditional approach.

4.3.1. LR workshop vessel

To test the method of including the roughness by changing the wall functions, a second vessel is studied. For the second vessel the rate of revolution of the propeller was predefined by the LR workshop and the workshop participants submitted, among other results, the speed and power, without knowing the measured speed and power. The comparison of the CFD calculations and speed trial measurements are shown in

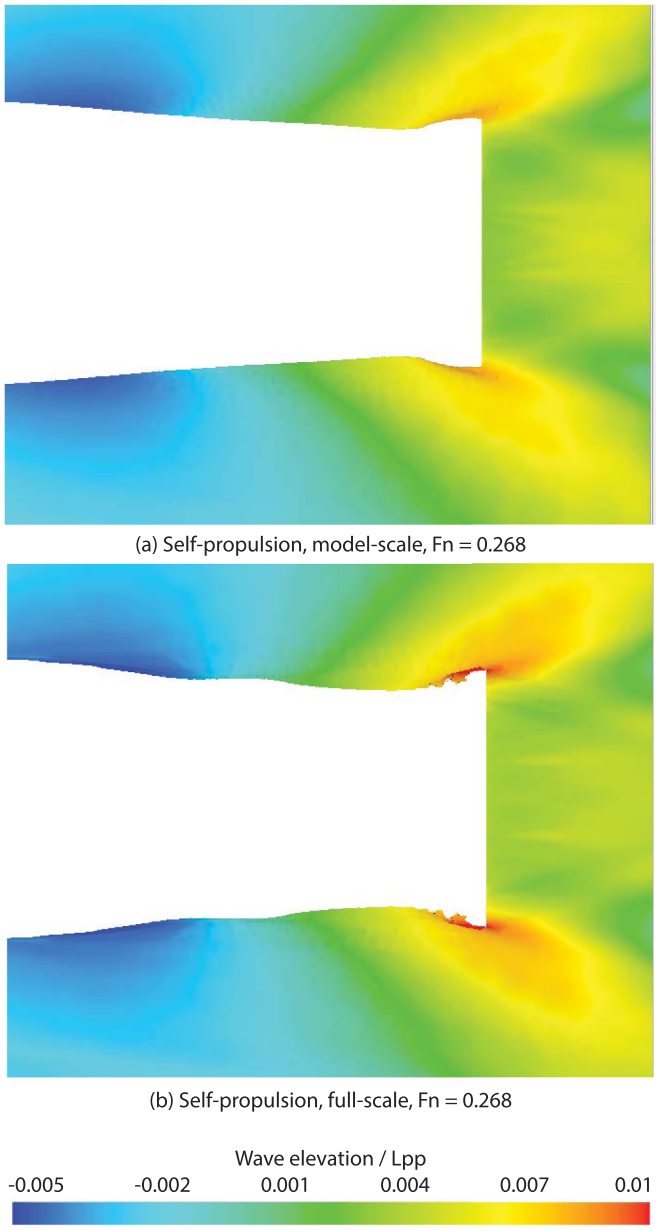

Fig. 10. Wave elevation non-dimensionalized with length between perpendiculars at aft seen from top. The hull and propellers are smooth for all shown conditions.

Fig. 1. It can be seen that the scatter of the CFD results are increasing when the RPM is increasing. Since the scatter at Fn = 0.182 is quite large, only the speed range of Fn = 0.140–0.168 is considered in this study. It can be seen that CFD results from some participants are very similar to the speed trial measurements and some are far off. The host of the workshop calculated a mean curve of the CFD results showing that the CFD simulations are under-predicting the power with up to 11.7%. This is consistent with the CFD results for ro-ro vessel, when using the empirical Townsin roughness approach.

By using the self-propulsion set-up described in Sec. 3.4.2, CFD calculations have been conducted for the three fixed speeds Fn = 0.140, Fn = 154, and Fn = 0.168. The mesh validated for the ro-ro vessel has been adapted to the REGAL vessel, and a mesh convergence study was conducted for the vessel showing a smaller spatial discretization error than for the ro-ro vessel cf. Table 17. A time step corresponding to two degrees of propeller rotation is used for the general cargo vessel. Since the vessel only has one propeller, both sides of the vessel are included in

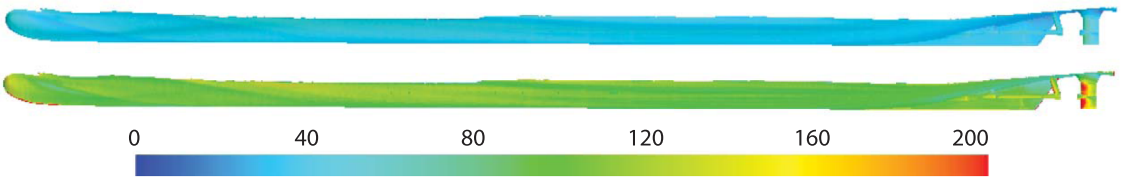

Fig. 11. R_S^+ (top) and wall y^+ (bottom) on the wetted surface of the ro-ro vessel with $R_S = 120\mu m$ at Fn = 0.245.

the CFD simulations. The discrepancies between the speed trial measurement and both the CFD from the LR Workshop participants and CFD conducted by the authors using the Townsin empirical roughness are shown in Table 19. It is seen that the results of the present CFD simulations using the empirical Townsin roughness approach provide results similar to the LR Workshop mean curve. In both cases the power is underestimated by 10–14%.

CFD simulations are now conducted for the general cargo vessel, where the roughness is taken into account using the modified wall functions. Unfortunately, the roughness of the hull and propeller is unknown. It is assumed that the roughness of the propeller is $R_s = 30\mu m$. Three different hull roughness heights are tested in the range of $R_s = 100\mu m$–$150\mu m$ based on the literature study presented in Sec. 3.3. The discrepancies between the CFD results and speed trial measurement are shown in Fig. 13. Using this approach the power is underestimated with 6.1–11.1% for $R_s = 100\mu m$ and with $3.1 - 0.1\%$ for $R_s = 150\mu m$. These discrepancies are generally smaller than when using the empirical Townsin roughness approach. The speed dependence tendency is clearly seen in Fig. 13. For the lowest to highest speed there is an approximately 5 percentage points off-set. The monotonic behaviour of the speed dependence for the general cargo vessel is not observed for the ro-ro vessel in Fig. 9. The offset of approximately 5 percentage points is believed to come from other uncertainty contributors that roughness as discussed in Sec. 4.2.3.

The larger underestimation of for the general cargo vessel than for the ro-ro vessel could indicate that the surface roughness of the general cargo vessel is larger than for the ro-ro vessels, even though the ro-ro vessels have been in the water longer time before the speed trial. Since the general cargo vessel is an older vessel with multiple previous dry dockings in its history, the paint roughness is potentially higher as seen in Table 3 where the results from Atencio and Chernoray [37] show that old underlying roughness accumulated from many dry dockings can have a large impact on the roughness height. However, it is important to remember that modelling of roughness is only one of the discrepancy contributors. The trend of higher accuracy when including the roughness of the hull and propeller instead of using the Townsin roughness allowance is similar for both the low block ro-ro vessel and the high block general cargo vessel. This gives the clear indication that including the roughness by modifying the wall functions can significantly improve the accuracy of the CFD simulation.

Table 19
Discrepancy in delivered power between LR speed trial measurements and CFD calculations both from LR workshop mean curve and present CFD results using the ITTC roughness.

Froude number	0.140	0.154	0.168
LR workshop mean	− 11.7%	− 10.5%	− 11.1%
Present CFD results	− 13.8%	− 12.4%	− 13.1%

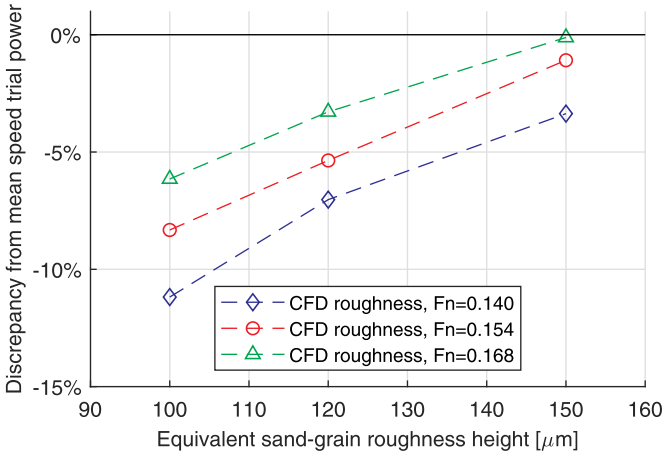

Fig. 13. Discrepancy of CFD results compared to delivered power from speed trials as function of hull roughness height for the LR workshop vessel REGAL.

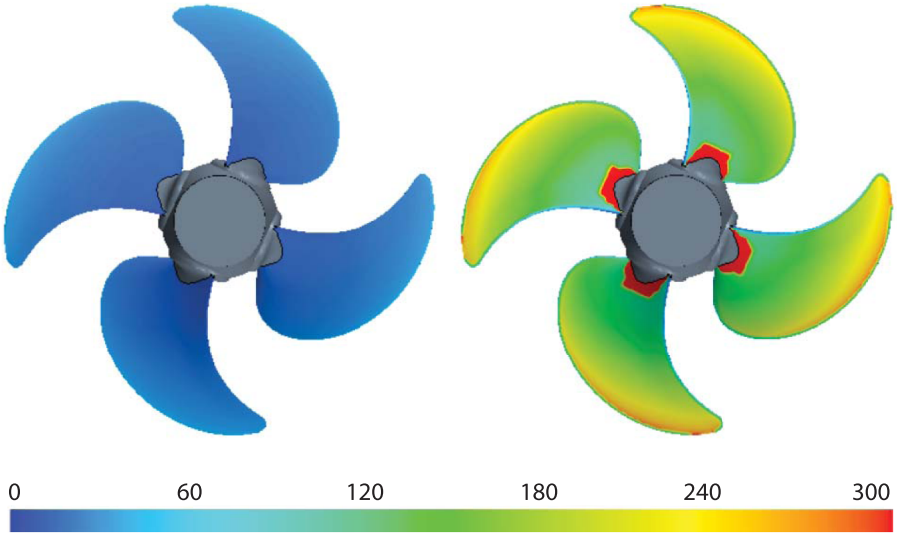

Fig. 12. R_S^+ (left) and wall y^+ (right) on the ro-ro vessel propeller with $R_S = 30\mu m$ at Fn = 0.245.

5. Conclusions

A full-scale self-propulsion CFD set-up with free surface and rotating propeller has been developed and verified and validated in systematic steps in order to ensure accuracy. The reference in full-scale was the mean speed/power curve from speed trials of the six sister vessels. The scatter of the speed trials was small with most of the measurements within 3% of the mean curve. The towing tank prediction of the delivered power in full-scale was within 1% of the speed trial for all speeds. Due to this excellent accuracy of the towing tank prediction, the towing tank measurements and predictions were used to validate the CFD set-up in systematic steps. The discrepancies for resistance, propeller open-water and model scale self-propulsion CFD simulations were found to be within the model test uncertainty. However, for the full-scale self-propulsion simulation, the delivered power from CFD was underestimated with 8–12% compared to the speed trial measurements when the roughness was estimated using the standard empirical formula by Townsin and applied as a point force in the center of gravity. By including a roughness model directly into the self-propulsion simulation using a modifying wall function approach, the discrepancy was significantly reduced. The same conclusions were found for a general cargo vessel where the geometry and speed trial data are publicly available. Unfortunately, the exact roughness of the surface of the two vessels was unknown. Based on a literature study on roughness measurements on newly painted ships, a range of sand-grain equivalent roughness heights of 100–150μm was tested for both vessels resulting in significantly reduced discrepancies to the speed trial measurements for both cases. This indicates that using a roughness model directly into the CFD simulation is more accurate than the traditional method using empirical formulas designed for towing tanks.

CRediT authorship contribution statement

Henrik Mikkelsen: Conceptualization, Methodology, Software, Validation, Formal analysis, Investigation, Writing - original draft, Writing - review & editing, Visualization, Funding acquisition. **Jens Honoré Walther:** Conceptualization, Methodology, Writing - review & editing, Supervision, Project administration, Funding acquisition.

Declaration of Competing Interest

The authors declare that they have no known competing financial interests or personal relationships that could have appeared to influence the work reported in this paper.

Acknowledgements

The research was supported by The Danish Maritime Fund under grant 2018-11, whose support is greatly appreciated. We would like to thank the shipyard and propeller manufacturer for providing unique and rarely shared data.

References

[1] IMO, Amendments to marpol annex vi on regulations for the prevention of air pollution from ships by inclusion of new regulations on energy efficiency for ships, MEPC 62/24/Add.1, Annex 19, 2011.
[2] J. Kim, I.-R. Park, K.-S. Kim, S.-H. Van, Numerical simulation of turbulent free surface flow around a self-propelled ship, Proc. Fifteenth Int. Offshore Polar Eng. Conf., Seoul, Korea, (2005), pp. 180–186.
[3] L. Larsson, F. Stern, M. Visonneau, Proceedings of Gothenburg 2010 - A workshop on numerical ship hydrodynamics, (2010).
[4] L. Larsson, F. Stern, M. Visonneau, T. Hino, N. Hirata, J. Kim, Proceedings of Tokyo 2015 workshop on CFD In Ship hydrodynamics, (2015).
[5] D. Ponkratov, Proceedings of 2016 workshop on ship scale hydrodynamic computer simulation, Lloyd's Register, 2017.
[6] H. Jasak, V. Vukčević, I. Gatin, I. Lalović, CFD validation and grid sensitivity studies of full scale ship self propulsion, Int. J. Nav. Archit. Ocean Eng. 11 (1) (2019) 33–43, https://doi.org/10.1016/j.ijnaoe.2017.12.004.
[7] H. Mikkelsen, M.L. Steffensen, C. Ciortan, J.H. Walther, Ship scale validation of CFD model of self-propelled ship, Mar. 2019 Comput. Methods Mar. Eng. VIII, (2019), pp. 718–729.
[8] W. Sun, Q. Hu, S. Hu, J. Su, J. Xu, J. Wei, G. Huang, Numerical Analysis of Full-Scale Ship Self-Propulsion Performance with Direct Comparison to Statistical Sea Trail Results, J. Mar. Sci. Eng. 8 (1) (2020) 24, https://doi.org/10.20944/preprints201912.0318.v1.
[9] T. Cebeci, P. Bradshaw, Momentum transfer in boundary layers, Hemisphere Publishing Corporation/McGraw-Hill, 1977.
[10] S. Song, Y.K. Demirel, M. Atlar, An investigation into the effect of biofouling on the ship hydrodynamic characteristics using CFD, Ocean Eng. 175 (2019) 122–137, https://doi.org/10.1016/j.oceaneng.2019.01.056.
[11] S. Song, Y.K. Demirel, M. Atlar, O. Turan, Validation of the CFD approach for modelling roughness effect on ship resistance, 6th Int. Conf. Adv. Model Meas. Technol. Marit. Ind. (2019).
[12] S. Song, Y.K. Demirel, M. Atlar, Penalty of hull and propeller fouling on ship self-propulsion performance, Appl. Ocean Res. 94 (2020) 102006, https://doi.org/10.1016/j.apor.2019.102006.
[13] IMO, ISO 15016:2015, MEPC 68/INF.14 (2015).
[14] Siemens, STAR-CCM+ User guide, Version 2019.1.1, 2019.
[15] J. Ferziger, M. Peric, Computational methods for fluid dynamics, 3rd Edition, Springer, 2002.
[16] D. Wilcox, Turbulence modelling for CFD, 2nd edition, DCW. Industries, 1998.
[17] T.-H. Shih, W.W. Liou, A. Shabbir, Z. Yang, J. Zhu, A new k-ϵ eddy viscosity model for high Reynolds number turbulent flows, Comput. Fluids 24 (3) (1995) 227–238, https://doi.org/10.1016/0045-7930(94)00032-T.
[18] R.B. Langtry, A correlation-based transition model using local variables for unstructured parallelized CFD codes, University of Stuttgart, 2006 Ph.D. thesis.
[19] C. Hirt, B. Nichols, Volume of fluid (VOF) method for the dynamics of free boundaries, J. Comput. Phys. 39 (1) (1981) 201–225, https://doi.org/10.1016/0021-9991(81)90145-5.
[20] S. Muzaferija, M. Peric, Computation of free-surface flows using the finite-volume method and moving grids, Numer. Heat Transf. Part B Fundam. 32 (4) (1997) 369–384, https://doi.org/10.1080/10407799708915014.
[21] I.B. Celik, U. Ghia, P.J. Roache, C.J. Freitas, H. Coleman, P.E. Raad, Procedure for estimation and reporting of uncertainty due to discretization in CFD applications, J. Fluids Eng. 130 (7) (2008) 078001, https://doi.org/10.1115/1.2960953.
[22] L.F. Richardson, The approximate arithmetical solution by finite differences of physical problems involving differential equations, with an application to the stresses in a masonry dam, Philos. Trans. R. Soc. A Math. Phys. Eng. Sci. 210 (459-470) (1910) 307–357, https://doi.org/10.1098/rsta.1911.0009.
[23] L.F. Richardson, J.A. Gaunt, The deferred approach to the limit. Part I. Single lattice. Part II. Interpenetrating lattices, Philos. Trans. R. Soc. A Math. Phys. Eng. Sci. 226 (636-646) (1927) 299–361, https://doi.org/10.1098/rsta.1927.0008.
[24] P.J. Roache, Verification of codes and calculations, AIAA J. 36 (5) (1998) 696–702.
[25] B.S. Bowden, N.J. Davison, Resistance increments due to hull roughness associated with form factor extrapolation methods, Natl. Phys. Lab. Sh. Tech. Man. 3800 (1974).
[26] ITTC, 1978 ITTC - Performance prediction method. ITTC - Recommended procedures and guidelines, Procedure 7.5-02-03-01.4, Revision 01, 2008.
[27] R.L. Townsin, M.A. Mosaad, The ITTC line its genesis and correlation allowance, Nav. Archit. 1985 (1985).
[28] ITTC, The propulsion commitee - Final report and recommendations to the 28th ITTC, Proc. 28h ITTC, 2017 1 (2017).
[29] F.H. Clauser, Turbulent boundary layers in adverse pressure gradients, J. Aeronaut. Sci. 21 (2) (1954) 91–108, https://doi.org/10.2514/8.2938.
[30] Y.K. Demirel, O. Turan, A. Incecik, Predicting the effect of biofouling on ship resistance using CFD, Appl. Ocean Res. 62 (2017) 100–118, https://doi.org/10.1016/j.apor.2016.12.003.
[31] M.P. Schultz, K.A. Flack, The rough-wall turbulent boundary layer from the hydraulically smooth to the fully rough regime, J. Fluid Mech. 580 (2007) 381–405, https://doi.org/10.1017/S0022112007005502.
[32] M. Leer-Andersen, L. Larsson, An experimental/numerical approach for evaluating skin friction on full-scale ships with surface roughness, J. Mar. Sci. Technol. 8 (1) (2003) 26–36, https://doi.org/10.1007/s10773-003-0150-y.
[33] J. Nikuradse, Stromungsgesetze in rauhen rohren. Forsch, Arb. Ing.-Wes., 361, English Transl. as NACA-TM-1292 3 (1933).
[34] A. Lindholdt, K. Dam-Johansen, S.M. Olsen, D.M. Yebra, S. Kiil, Effects of biofouling development on drag forces of hull coatings for ocean-going ships: a review, J. Coatings Technol. Res. 12 (3) (2015) 415–444, https://doi.org/10.1007/s11998-014-9651-2.
[35] I.K.A.P. Utama, B. Nugroho, C. Chin, M.L. Hakim, F.A. Prasetyo, M. Yusuf, I.K. Suastika, J. Monty, N. Hutchins, B. Ganapathisubramani, A study of skin friction-drag from realistic roughness of a freshly cleaned and painted ship hull, Proc. Int. Symp. Mar. Eng. (2017).
[36] M.P. Schultz, Frictional resistance of antifouling coating systems, J. Fluids Eng. 126 (6) (2004) 1039–1047, https://doi.org/10.1115/1.1845552.
[37] B. Niebles Atencio, V. Chernoray, A resolved RANS CFD approach for drag characterization of antifouling paints, Ocean Eng. 171 (2018) (2019) 519–532, https://doi.org/10.1016/j.oceaneng.2018.11.022.
[38] M.P. Schultz, J.M. Walker, C.N. Steppe, K.A. Flack, Impact of diatomaceous biofilms on the frictional drag of fouling-release coatings, Biofouling 31 (9) (2015) 759–773, https://doi.org/10.1080/08927014.2015.1108407.
[39] O. Usta, E. Korkut, A study for the effect of surface roughness on resistance characteristics of flat plates, Int. Conf. Mar. Coatings, Royal Institution of Naval Architects, 2013, pp. 29–37.

[40] D. Howell, B. Behrends, A review of surface roughness in antifouling coatings illustrating the importance of cutoff length, Biofouling 22 (6) (2006) 401–410, https://doi.org/10.1080/08927010601035738.
[41] D. Owen, Y.K. Demirel, E. Oguz, T. Tezdogan, A. Incecik, Investigating the effect of biofouling on propeller characteristics using CFD, Ocean Eng. 159 (2018) 505–516, https://doi.org/10.1016/j.oceaneng.2018.01.087.
[42] T. Adams, C. Grant, H. Watson, A simple algorithm to relate measured surface roughness to equivalent sand-grain roughness, Int. J. Mech. Eng. Mechatronics 1 (1) (2012) 66–71, https://doi.org/10.11159/ijmem.2012.008.
[43] M.P. Schultz, Effects of coating roughness and biofouling on ship resistance and powering, Biofouling 23 (5) (2007) 331–341, https://doi.org/10.1080/08927010701461974. arXiv:1011.1669v3
[44] ITTC, ITTC Recommended procedures and guidelines - Practical guidelines for ship self-propulsion CFD, 2014.
[45] L. Eça, M. Hoekstra, Numerical aspects of including wall roughness effects in the SST k-epsilon eddy-viscosity turbulence model, Comput. Fluids 40 (1) (2011) 299–314, https://doi.org/10.1016/j.compfluid.2010.09.035.